NJC

Accepted Manuscript

This article can be cited before page numbers have been issued, to do this please use: H. G. Bonacorso, T. P. Calheiro, B. A. Iglesias, T. Acunha, S. Franceschini, A. Ketzer, A. R. Meyer, L. V. Rodrigues, P. A. Nogara, J. B. T. Rocha, M. A. P. Martins and N. Zanatta, *New J. Chem.*, 2017, DOI: 10.1039/C7NJ04032F.

ROYAL SOCIETY OF CHEMISTRY

rsc.li/njc

View Article Online
DOI: 10.1039/C7NJ04032F

Journal Name

ARTICLE

1,1-Difluoro-3-aryl(heteroaryl)-1*H*-pyrido[1,2-*c*][1,3,5,2]oxadiazaborinin-9-ium-1-uides: Synthesis; structural characterization; and photophysical, electrochemical, and BSA-binding studies

17Received 00th January 20xx,
Accepted 00th January 20xx

DOI: 10.1039/x0xx00000x

www.rsc.org/

Helio G. Bonacorso,[a]* Tainara P. Calheiro,[a] Bernardo A. Iglesias,[b]* Thiago V. Acunha,[b] Steffany Z. Franceschini,[a] Alex Ketzer,[a] Alexandre R. Meyer,[a] Letícia V. Rodrigues,[a] Pablo A. Nogara,[c] João B. T. Rocha,[c] Nilo Zanatta,[a] and Marcos A. P. Martins [a]

This paper presents a series of six examples of 1,1-difluoro-3-aryl(heteroaryl)-1*H*-pyrido[1,2-*c*][1,3,5,2]oxadiazaborinin-9-ium-1-uides (**2**) — in which aryl(heteroaryl) = phenyl, 4-MeC_6H_4, 4-N$(CH_3)_2C_6H_4$, 4-NO_2C_6H4, 2-naphthyl, and 2-thienyl — as pyridine-based boron heterocycles with variable ligand structures. The heterocycles **2** were easily synthesized at yields of 51–70 % from reactions — at room temperature for 24 h — of simple *N*-(pyridin-2-yl)benzamides (**1**) with $BF_3{\cdot}Et_2O$, and they were fully characterized by ^{1}H-, ^{13}C-, ^{19}F-, and ^{11}B-NMR, GC–MS, and X-ray diffractometry. The optical and electrochemical properties of **2** (UV–vis, fluorescence, quantum yield calculations, Stokes shift, redox potential, and DFT calculations) were determined and discussed. BSA-binding experiments and molecular docking studies of new complexes **2** were performed and correlated between each other.

Introduction

Fluorescent organoboron compounds have been extensively explored in recent years, and their photophysical properties have been utilized in many fields of current research. Among boron complexes, boron-dipyrromethene (BODIPY) and its derivatives have excellent fluorescence properties; for example, outstanding fluorescence quantum yields, sharp absorption and fluorescence spectra, and high chemical stability.[1]

The optical and physical properties of boron complexes and their derivatives have been explored in energy conversion devices (organic light-emitting diodes and organic photovoltaics),[2–4] energy transport devices,[5] solar concentrators,[6] and NIR-absorbing systems.[7] All these features are beneficial for the spectroscopic properties inducing well-defined and sharp absorption and emission transitions, high quantum yields, and suitable excited-state lifetimes.[8] Additionally, many nitrogenated heterocyclic scaffolds like pyridine (I, II), quinoxalines (III), and 1,8 naphthyridines (IV) have also been explored in the synthesis of similar compounds (Figure 1).

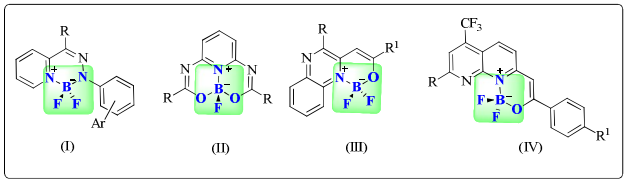

Fig 1. Examples of compounds containing a BF_2 core.

Compounds like the ones shown in Figure 1 have widespread applications; for example, in chemosensors,[9] biomolecular labeling,[10] and photodynamic therapy.[11] Recent research has also described the use of these structures as fluorescence lifetime probes for DNA interactions.[12] Additionally, bovine serum albumin (BSA) has been used as a model protein in research, due to its high stability, low cost, and similar structure to human serum albumin. The interaction between dyes and BSA changes the fluorescent signal of dyes, thus providing a convenient method to achieve the detection of BSA.[13]

Recently Grabarz[14] and Bednarska[15] reported the synthesis of similar pyridine systems using cyclic and acyclic unsaturated chains, as π-conjugated spacer moieties, binding a dimethyl amino group to the difluoroboranyl structures in order to evaluate their photochemical properties. However, there is a lack for understanding of the electronic effects on the

[a] *Núcleo de Química de Heterociclos (NUQUIMHE), Departamento de Química, Universidade Federal de Santa Maria, Santa Maria 97105-900, Brazil. E-mail: helio.bonacorso@ufsm.br*
[b] *Departamento de Química, Universidade Federal de Santa Maria, Santa Maria, RS 97105-900, Brazil. E-mail: bernardopgq@gmail.com*
[c] *Laboratório de Bioquímica Toxicológica, Departamento de Bioquímica e Biologia Molecular, Universidade Federal de Santa Maria, 97105-900, Santa Maria-RS, Brazil*

† Electronic Supplementary Information (ESI) available: [details of any supplementary information available should be included here]. See DOI: 10.1039/x0xx00000x

View Article Online
DOI: 10.1039/C7NJ04032F

photophysical and electrochemical properties, as well as BSA-binding studies for specific 3-aryl(heteroaryl)-substituted scaffolds. In this way, we firstly developed the synthesis under mild conditions (room temperature) for a series of fluoro-organoboron compounds (**2**) containing the pyridine ring, starting from BF_3OEt_2 and selected *N*-(pyridin-2-yl)benzamides (**1**). Amide **1** were previously described by Devi[16] as simple but useful building blocks. After the synthesis of the fluorinated heterocycles **2**, we conducted studies to evaluate the optical and electrochemical properties, as well as theoretical calculations. Additionally, BSA binding assays and a molecular docking study were done.

Results and discussion

Synthesis

The 1,1-difluoro-3-aryl(heteroaryl)-1*H*-pyrido[1,2-*c*][1,3,5,2]oxadiazaborinin-9-ium-1-uides (**2a–f**) were prepared using the *N*-(pyridine-2-yl)benzamides (**1a–f**) previously synthesized in accordance with the procedure described in the literature.[16] The benzamides (**1a–f**) were obtained from the reaction of 2-aminopyridine with the respective aldehydes, using aqueous hydrogen peroxide and water. Subsequently, starting from the procedures previously described in the literature,[17,18] the benzamides **1a–f** were subjected to the optimized reaction conditions, with $BF_3{\cdot}Et_2O$ in anhydrous chloroform at room temperature for 24 h, using triethylamine as base, which furnished the desired fluorine–boron compounds **2a–f** at satisfactory to good yields (51–70 %). The synthetic route, yields, and the structures of the synthesized four-coordinated organo-boron compounds **2** are shown in Table 1.

Table 1 Synthesis of 1,1-difluoro-3-aryl(heteroaryl)-1*H*-pyrido[1,2-*c*][1,3,5,2]oxadiazaborinin-9-ium-1-uides.[a,b]

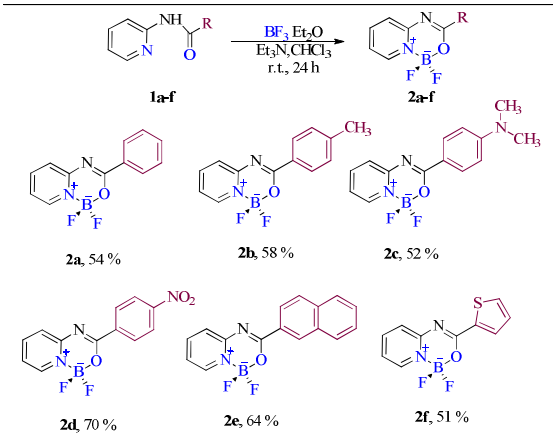

[a] Reaction conditions: *N*-(pyridin-2-yl)benzamides **1a-f** (3 mmol), $BF_3{\cdot}Et_2O$ (49 mmol, 6.0 mL), anhydrous triethylamine (32 mmol, 4.5 mL), anhydrous chloroform (60 mL), room temperature, 24 h. [b] Isolated yields after column chromatography.

The new organoboron compounds **2a–f** were obtained without decomposition, as yellow or white air-stable solids, with melting points in the range of 142–145 °C (**2f**) to 200–202 °C (**2e**).

In Table 1 it can be seen that the best yields for the series of **2a–f** were obtained for complexes containing a substituent with a strong electron-withdrawing group (–R) — for example, **2d** (R = 4-$NO_2C_6H_4$ at 70% yield); while the lowest yield was observed for the complex containing the electron-donating group (+R) — that is, **2f** (R = 2-thienyl at 51% yield).

Specific details of the experimental procedures and complete data for structural characterization via NMR and GC–MS are described in the supplementary material.

The new structures of **2** were confirmed and characterized by ^{1}H-, ^{13}C-, ^{11}B-, and ^{19}F-NMR, and their purity was evaluated from CHN elemental analysis. The structural assignments for synthesized benzamides **1a–f** are consistent with the ^{1}H- and ^{13}C-NMR spectra described in the literature for these compounds.[16] Thus, upon comparing the ^{1}H- and ^{13}C-NMR data of the benzamide precursors **1** with the new oxadiazaborinin derivatives 2, no significant differences were seen in the chemical shift values.

A comparison between the ^{1}H-NMR data of compounds **2a–f** and **1a–f** showed that the major evidence for the formation of compounds **2** was the signal disappearance of the hydrogen atom bonded to the nitrogen atom (N-H) in **1**, at 8.60–8.84 ppm.

Also, in order to demonstrate the formation of the BF_2 complexes, ^{19}F- and ^{11}B-NMR experiments were performed. In the $CDCl_3$ spectra for compounds **2a–f**, the ^{19}F-NMR showed a distorted quartet for each compound, with a broad base on average at -138.80 ppm (-139.62 to -137.95 ppm), which is in agreement with similar compounds described in the literature.[17,19] In the ^{11}B-NMR spectra, the ^{11}B signals for the series of compounds appear as a well-defined triplet for each compound, due to the coupling with the two ^{19}F nuclei. The chemical shifts for the boron atoms were observed on average at 0.50 ppm (0.37 to 0.65 ppm), with a coupling constant average of 13 Hz, which is due to the coupling between the atoms of boron and fluorine.

Finally, and in order to determine the real molecular structure of the compounds of series **2** in solid state, a single crystal X-ray diffraction measurement was performed for the BF_2 compound **2b** (Figure 2).

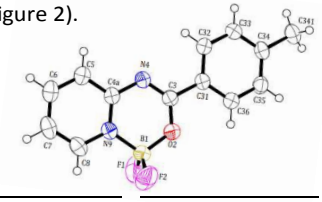

Bond length (Å)	Bond angles
B1- F1 = 1.351	B1-F1-O2 = 110.37°
B1- F2 = 1.352	F2-B1-O2 = 109.75°
B1- O2 = 1.440	F1-B1-N9 = 108.54°
B1- N9 = 1.567	F2-B1- N9 = 108.92°
O2- C3 = 1.310	N9-B1-O2 = 108.82°
C3- N4 = 1.288	F1-B1-F2 = 110.41°

Fig 2. ORTEP and selected lengths and bond angles of organoboron compound **2b** (CCDC 1529635).[20] Displacement ellipsoids are drawn at the 50% probability level, and H atoms are represented by circles with arbitrary radii.

View Article Online
DOI: 10.1039/C7NJ04032F

The crystals of compound **2b** were obtained by slowly evaporating a dichloromethane solution at room temperature. Compound **2b** was crystallized in a monoclinic lattice without solvates. The central B-atom has a slightly distorted tetrahedron geometry, with B-F, B-N, and B-O distances of 1.352, 1.567 and 1.440 Å, respectively, and bond angles around the B-atom ranging from 108.54° (F1-B1-N9) to 110.41° (F1-B1-F2). These values for bond lengths and bond angles are normal for similar fluoro-organoboro heterocycles.[21]
The dihedral angle between the atoms N(4)-C(3)-C(31)-C(32) had a torsion angle of 1.9 (2)°, which suggests that the oxazaborinine ring and the *p*-toluoyl substituent are almost in a periplanar orientation. The detailed crystallographic data are summarized in the supplementary material.

General absorption and emission properties of organoboron compounds 2a–f

The comparative absorption spectra of compounds **2a–f**, using chloroform as solvent, are shown in Figure 3. The optical properties are listed in Table 2. The absorption in the organoboron derivatives **2** indicates bands as follows: at 260–300 nm in the UV region, which can be attributed to the transition band of the intraligand π→π*; and the other at 310–410 nm, which can be attributed to the n→π* transition. It can be seen that the band shifts occur due to the electronic properties of the substituents present in the molecules. As an example, for compounds with substituent R = 4-$NMe_2C_6H_4$ (e.g., **2c**), a red shift is seen, contrary to what is observed for derivative **2a** (R = C_6H_5) and **2d** (R = 4-$NO_2C_6H_4$ — see Figure 3). These facts can be attributed to: the withdrawing effect of the π-electronic conjugation and the internal resonance (**2d** as a nitro group).

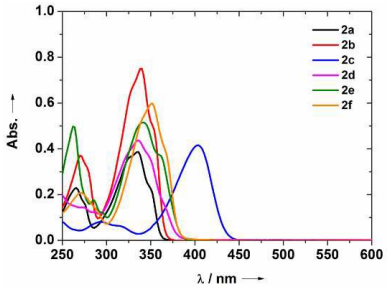

Fig 3. Comparative electronic UV-vis absorption spectra of organoboron complexes **2a–f** containing different substituent groups in $CHCl_3$ solutions.

The emission fluorescence spectra were recorded in N_2 saturated chloroform solution obtained by exciting the compounds **2a-f** at the absorption maxima wavelength of λ_{exc}= 340 nm (an average of the absorption bands between 330-350 nm). In general, the organoboron compounds exhibited emissions in the purple-blue region (400–460 nm range). As already observed in the ground state, they had locations comparable with the emission maxima, which indicates that different organic moieties in the organoboron complexes **2a–f** did not play a fundamental role in the excited state of these compounds. When the nature of the pyridyl-BF_2-type molecules in the excited state was compared, the same behaviour was observed in the emission spectra (Figure 4). These results can probably also be attributed to the nature of the π→π* intraligand electronic transition, which indicates that these compounds allow better electronic delocalization in the excited state.[16,19]

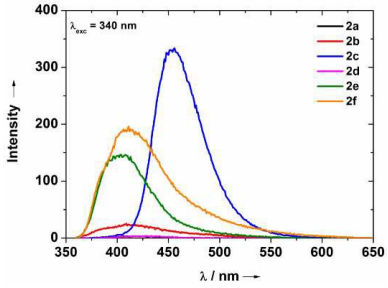

Fig. 4. Comparative emission spectra of organoboron complexes **2a–f** containing different substituent groups in $CHCl_3$ solutions at λ_{exc} = 340 nm.

The Stokes shifts observed in the excited state for these molecules indicate that boron derivatives show some charge separation (50–90 nm), which can be attributed to the intramolecular charge transfer character (ICT) in the excited state (Table 2).

Table 2. UV–vis and emission analysis data for compounds **2a–f.**

Comp.	λ, nm (ε, M^{-1} cm^{-1})[a]	λ_{em}, nm[b]	Φ_{fl}[c]	Stokes shifts (nm)[d]
2a	266 (1711), 324 (sh), 335 (2869), 351 (sh)	422	0.003	87
2b	271 (2740), 339 (5577), 353 (sh)	409	0.140	70
2c	293 (622), 317 (459), 403 (3074)	454	0.217	51
2d	274 (sh), 336 (3237)	423	< 0.001	87
2e	262 (3666), 286 (sh), 341 (3814), 362 (sh)	404	0.167	63
2f	271 (1540), 351 (4429)	411	0.176	60

sh = shoulder; [a]Measured in chloroform; [b]In chloroform (λ_{exc} = 340 nm); [c]9,10-Diphenylanthracene in $CHCl_3$ as standard (Φ_{fl} = 0.65); [d]$\Delta\lambda = \lambda_{em} - \lambda_{abs}$.

View Article Online
DOI: 10.1039/C7NJ04032F

The BF_2-derivatives **2a–f** had lower fluorescence quantum yields when compared to the 9,10-Diphenylanthracene quencher standard (Table 2). This suggests that the presence of the boron atom seems to be a non-efficient and non-radiative deactivation channel in these pyridyl-structure types.

Electrochemical behavior of organoboron complexes 2a–f

Cyclic voltammetry analysis of derivatives **2a–f** was recorded in 0.1 M $TBAPF_6$ CH_3CN solution with a glassy carbon electrode, using a platinum wire with a pseudo-reference electrode in acetonitrile, within a range of -1.50 to +2.00 V *versus* SHE (Figure 5 and Table 4). The CV data is referenced to the standard internal Fc/Fc^+ (0.49 V vs. SHE in CH_3CN).

In general, the electrochemical behavior of the organoboron compounds **2a–f** indicates a reduction process in the -0.60 to -1.20 V range in the cathodic region, which can be attributed to the fact that the reduction in the core of the organoboron complexes in all of the structures probably forms π-anion radical species.[22] In almost all cases, the re-oxidation of the organoboron complexes is not observed, except for compound **2d** (R = 4-$C_6H_4NO_2$), which indicates the decomposition of the pyridine unit upon reduction.

In the positive range (anodic region), oxidation peaks were observed in compounds **2a–f**, within the +0.70 to +1.50 V potential range, which can be attributed to the π-radical cation species formation in the organoboron complexes.[23,24]

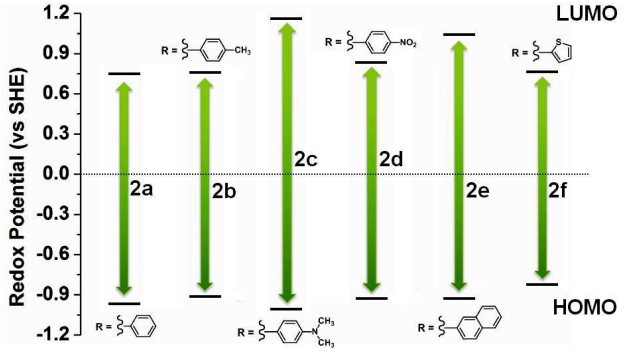

Fig. 5. Comparative redox potentials of compounds **2a–f** using $TBAPF_6$ as supporting electrolyte.

DFT calculations

For a better insight into the frontier orbitals of **2a–f**, DFT calculations were performed for these compounds with the Gaussian 09 package of programs.[25]

All geometrical structures were optimized at the SCRF(PCM)-B3LYP/cc-pVTZ level of theory, with the single point energies and molecular orbitals calculated at the TD-DFT-B3LYP/cc-pVTZ level of theory.

The data in Table 3 show the HOMO and LUMO density of compounds **2a–f**. Most of the compounds had the HOMO and LUMO densities distributed internally throughout each molecule; however, for compounds **2c** and **2e** it was seen that the HOMO density is located on the dimethylaminophenyl and naphthyl substituents, respectively. The theoretical UV-Vis spectra and related data (Table S3 and Figure S13 supplementary material) are in agreement with the experimental values.

Table 3. Energy and HOMO-LUMO density plots for **2a-f.**

Comp.	HOMO	LUMO	Energy (eV)
2a	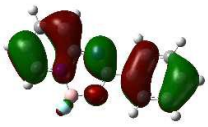	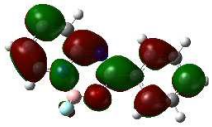	3.867
2b	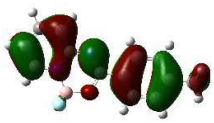	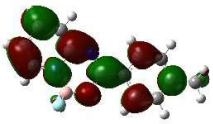	3.781
2c	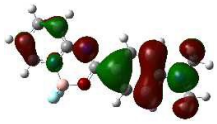	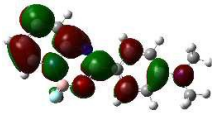	3.070
2d	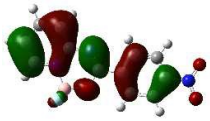	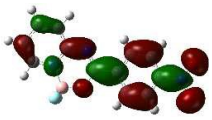	3.440
2e	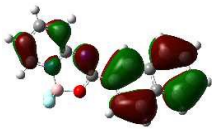	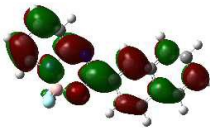	3.340
2f	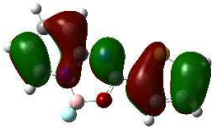	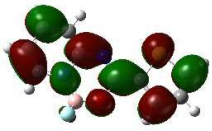	3.653

BSA binding assays

The electronic spectra of BSA in the absence and presence of the organoboron derivatives **2a–f** are shown in Figure 7 and in the Supplementary data. For free BSA, the peak observed at 280 nm corresponds to the absorption of tryptophan and tyrosine residues.[26] The enhancement, upon addition of the boron-complexes, in the BSA's absorption band at 280 nm indicated that these compounds bind to the protein.

View Article Online
DOI: 10.1039/C7NJ04032F

Table 4. Electrochemical data for compounds **2a–f**.

Comp.	R	E_1 (V)	E_2 (V)	E_3 (V)	E_4 (V)	$E_{0\text{-}0}$[d]	HOMO[e]	LUMO[f]
2a	C_6H_4	-0.970[a]	+0.752[b]	+1.353[b]	-----	3.254	-5.552	-2.298
2b	4-$CH_3C_6H_4$	-0.917[a]	+0.755[b]	+1.309[b]	-----	3.444	-5.555	-2.111
2c	4-$NMe_2C_6H_4$	-1.013[a]	+1.153[b]	+1.266[b]	+1.406[b]	3.297	-5.953	-2.656
2d	4-$NO_2C_6H_4$	-0.638[c]	-0.930[a]	+0.833[b]	+1.448[b]	3.212	-5.633	-2.421
2e	2-Naphtyl	-0.931[a]	-1.197[c]	+1.039[b]	-----	3.434	-5.839	-2.405
2f	2-Thienyl	-0.828[a]	+0.759[b]	+1.299[b]	-----	3.454	-5.559	-2.105

[a]E_{pc} = cathodic peak; [b]E_{pa} = anodic peak; [c]$E_{1/2} = E_{pc} + E_{pa} / 2$; [d]Determined from the interception of the normalized absorption and emission spectra ($E_{0\text{-}0} = 1240/\lambda_{intercp}$ in eV); [e]E_{HOMO} = - [4.8 + 1[st]E_{ox} (vs. SHE)]eV; [f]$E_{LUMO} = [E_{HOMO} + E_{0\text{-}0}]$eV

View Article Online
DOI: 10.1039/C7NJ04032F

Journal Name

ARTICLE

The electronic spectral change of BSA upon incremental addition of these molecules may reflect the change in the environment of the amino acid residues; that is, the conformational changes that occur upon binding with these compounds. Such a significant variation in the electronic spectra of BSA indicates that these compounds bind to BSA to form a complex, which induces conformational changes in the BSA molecule.

The equilibrium (K_b) and quenching (K_{SV}) constants were evaluated from the linear plots of emission intensities versus organoboron complex concentration — the values obtained are shown in Table 5. The relatively high quenching (10^4 M^{-1} range) and binding constant values (10^4 to 10^5 M^{-1} range) obtained for the organoboron complexes suggests that there is a good interaction between the compounds and the BSA structure. As an example, compound **2e** exhibited the highest binding and quenching constant values (Figure 6). The number of binding sites n is close to 1, which suggests the presence of a single binding site for the compounds in the BSA molecule. All the BSA emission assays are shown in the Supplementary data.

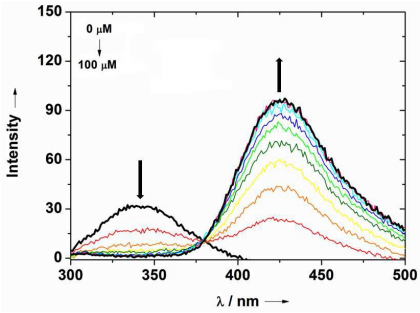

Fig. 6. Fluorescence quenching emission spectra of BSA in the absence and presence of compound **2e** (BSA = 1.0 μM and **2e** = 0 – 100 μM).

Table 5. Stern–Volmer quenching constant (K_{SV}), binding constant (K_b), and the number of binding sites (*n*) for the interactions of compounds with BSA.

Comp.	K_{SV} (M^{-1})	K_b (M^{-1})	*n*
2a	6.03×10^3	8.10×10^2	0.27
2b	8.59×10^3	1.37×10^3	0.21
2c	1.16×10^4	1.51×10^4	0.38
2d	5.24×10^4	1.46×10^4	0.25
2e	2.54×10^5	1.99×10^4	0.32
2f	1.80×10^5	1.77×10^4	0.21

Molecular docking of BSA

The blind docking simulation showed that most of the conformers of compounds **2** interact in the region close to Trp134. Thus, a local semi-flexible docking was done in the region around the Trp34 residue, with the lateral chain of the residues Arg185, Lys136, Lys131, Trp134, Tyr137 and Tyr160 flexible, in order to increase the interactions between ligand and protein.

The semi-flexible docking showed that the compounds that have the benzene ring (**2a–2d**) bind between two α-helix, interacting weakly with the Trp134. However, compounds **2e** and **2f** interact directly with the Trp134 residue, via π-π stacking between the imidazole ring of Trp134 and the 2-naphtyl and 2-thienyl substituents of the respective compounds **2** (Figure 7).

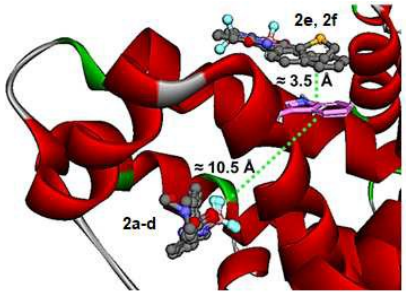

Fig. 7. Binding sites of the organoboron complexes with the BSA.

A conformation pattern was observed for compounds **2a–d**, which indicates that the substituents in the benzene ring do not change the orientation of the molecules in the BSA protein. On the other hand, compounds **2e** and **2f** — which have naphthalene and thiophene rings, respectively — interact with the Trp134.

Thus, correlating the values determined by the Stern-Volmer quenching and binding constants and the molecular docking, it could be seen that both experiments show the more

View Article Online
DOI: 10.1039/C7NJ04032F

pronounced interaction of tryptophan with compounds **2e** and **2f**. It is believed that this increased interaction occurs because of the stereochemistry of these compounds.

Conclusions

In summary, we firstly described the easy synthesis of 1,1-difluoro-3-aryl(heteroaryl)-1*H*-pyrido[1,2-*c*][1,3,5,2]oxadiazaborinin-9-ium-1-uides (**2**) — from very accessible benzamides **1** — at good yields. Compounds **2** are solid, air-stable, easy to handle, and could be fully characterized by ^{1}H-, ^{13}C-, ^{11}B- and ^{19}F-NMR spectroscopy and X-ray diffractometry. The pyridinyl-boron complexes showed small differences in emission fluorescence values for both electron-donating and electron-accepting groups. The DFT calculations showed HOMO and LUMO densities distributed throughout each molecule; however, compounds **2c** and **2e** had HOMO densities distributed over the 4-dimethylaminophenyl and 2-naphthyl substituents, respectively. The results of the BSA-binding studies for compounds **2e** (2-naphthyl substituted) and **2f** (2-thienyl substituted) indicated that the greatest interaction was with the tryptophan site.

Experimental section

Unless otherwise indicated, all common reagents and solvents were used as obtained from commercial suppliers, without further purification. ^{1}H- and ^{13}C-NMR spectra were acquired on Bruker Avance III 400 MHz spectrometers for one-dimensional experiments, with 5 mm sample tubes, 298 K, and digital resolution of 0.01 ppm, in $CDCl_3$ as solvent and using TMS as the internal reference. The ^{19}F- and ^{11}B-NMR spectra were acquired on a Bruker Avance III (^{19}F at 564 MHz and ^{11}B at 192 MHz), equipped with a 5 mm PABBO probe, 5 mm sample tubes at 298 K, digital resolution of 0.01 ppm, in $CDCl_3$, and using $CFCl_3$ and $BF_3{\cdot}OEt_2$, respectively, as the external reference.

All results are reported with the chemical shift (δ), multiplicity, integration, and coupling constant (Hz). The following abbreviations were used to explain multiplicities: s = singlet, d = doublet, t = triplet, q = quartet, m = multiplet, and dd = double doublet. All NMR chemical shifts are reported in parts per million, relative to the internal reference. All melting points were determined using coverslips on a Microquímica MQAPF-302 apparatus and are uncorrected. The CHN elemental analyses were performed on a Perkin–Elmer 2400 CHN elemental analyzer (University of São Paulo, Brazil).

The reflections for the X-ray diffractometry were measured by using a D8 Venture, Bruker Photon CMOS Detector (MoKα radiation: λ = 0.71073 Å)[27] up to a resolution of (sin u/l)max = 0.60 Å1, at a temperature of 293 K. The structures were solved with SHELXS-2013[28] by using direct methods, and they were refined with SHELXL-201326 on F2 for all reflections. Non-hydrogen atoms were refined by using anisotropic displacement parameters. The positions of the hydrogen atoms were calculated for idealized positions. The structures were solved with SHELXS-2013 by using direct methods and refined with SHELXL-2013 on F2 for all reflections.

The molecular graph was prepared using ORTEP-3 for Windows.[29] The crystallographic data for the structure of **2b** have been deposited with the Cambridge Crystallographic Data Centre and allocated the deposition number CCDC 1529635. Copies of the data can be obtained free of charge upon application to: CCDC, 12 Union Road, Cambridge CB2 1EZ, UK (fax: +44 1223336033 or deposit@ccdc.com.ac.uk).

UV-vis absorption spectra were recorded on a Shimadzu UV2600 spectrophotometer, using chloroform as solvent. Emission spectra of samples in $CHCl_3$ and DMSO/PBS mixture solutions were measured with a Varian Cary 50 Eclipse fluorescence spectrophotometer (emission; slit 2.0 mm), and were corrected in accordance with the manufacturer's instructions. Fluorescence quantum yields (Φ_{fl}) of the compounds **2a–f** in solutions were determined by comparing the corrected fluorescence spectra with that of 9,10-Diphenylanthracene in chloroform (Φ_{fl} = 0.65) as the standard.[30]

Cyclic voltammograms were recorded on an AutoLab EcoChimie PGSTAT 32N potenciostat/galvanostat system, at room temperature under argon atmosphere, using dry acetonitrile solution (Sigma-Aldrich). Electrochemical grade tetrabutylammonium hexafluorophosphate (0.1 M, TBAPF6, Sigma-Aldrich) was used as supporting electrolyte. These experiments were performed using a standard three-component system: a glassy carbon working electrode, a platinum wire auxiliary electrode, and a platinum wire pseudo-reference electrode. For monitoring of the reference electrode, the Fc/Fc^{+} couple was used as an internal reference ($E_{1/2}$ = 0.46 V vs. NHE). All measurements were performed at room temperature (298 K).[31]

All theoretical calculations were performed with the Gaussian 09 package of programs.[25] The structures of the compounds were full optimized without any constrain at the B3LYP/cc-pVTZ level of theory. The PCM model was used for account the acetonitrile solvent effect. Harmonic frequencies calculations were performed with de aim to confirm that the geometries are on minimum of potential energy. UV-vis spectroscopic properties were obtained by TD-DFT single point calculations at the B3LYP/cc-pVTZ level and the acetonitrile solvent effects were accounted by the PCM model.

The 3D structure of BSA was obtained from the Protein Data Bank (http://www.rcsb.org/pdb/) with the following code: 4f5s.[32] The Chimera 1.8 software[33] was used to remove the chain B, waters, and other molecules, and also to add hydrogens to the BSA protein. The ligands were built in the Avogadro 1.1.1 software,[34] following the semi-empirical PM6[35] geometry optimization, using the MOPAC2012 program.[36] The ligands and protein were generated in the pdbqt format by Auto Dock Tools — the ligands were considered to be flexible (with PM6 charges) and the enzyme rigid (with Gasteiger charges).[37]

The Auto Dock Vina 1.1.1 program was used for the blind docking,[38] using a gridbox of 92 x 62 x 86 and the coordinates x

View Article Online
DOI: 10.1039/C7NJ04032F

= 9.457, y = 23.359, and z = 98.149, with an exhaustiveness of 50. Due to the Auto Dock not recognizing the B atom, it was replaced by C, in the *pdbqt* file. The semi-flexible docking was done in the region involving the Trp134 residue, with a gridbox of 30 x 30 x 35 and the coordinates x = 20.324, y = 33.690, and z = 97.801. The lateral chain of the residues Arg185, Lys136, Lys131, Trp134, Tyr137, and Tyr160 was considered flexible during the docking, in order to increase the interactions between ligand and protein. The conformer that interacts most closely with the Trp134 residue was selected. The results from the docking were analyzed using the Accelrys Discovery Studio 3.5 software.[39]

General procedure for the synthesis of *N*-(pyridin-2-yl)benzamides (1a–f)

The *N*-(pyridin-2-yl) benzamides were synthesized in accordance with the procedure described in the literature.[16]

General procedure for the synthesis of 1,1-difluoro-3-aryl(heteroaryl)-1*H*-pyrido[1,2-*c*][1,3,5,2]oxadiazaborinin-9-ium-1-uides (2a–f)

The BF_2 complexes **2** were synthesized using a procedure similar to that described in the literature.[17,18] Solutions of the respective *N*-(pyridin-2-yl)benzamides **1a–f** (3 mmol), $BF_3{\cdot}Et_2O$ (6.0 mL, 49 mmol), and anhydrous triethylamine (4.5 mL, 32 mmol) in anhydrous chloroform (60 mL) were magnetically stirred for 24 h at room temperature. At the end of the reactions (TLC), the resulting mixtures were extracted with dichloromethane (3 x 20 mL) and water (3 x 20 mL). The organic phase of each reaction was dried over anhydrous Na_2SO_4, and the solvent was evaporated under reduced pressure. The crude products **2a–f** were purified by column chromatography on silica gel 60, using dichloromethane as the eluent.

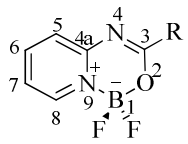

1,1-difluoro-3-phenyl-1*H*-pyrido[1,2-*c*][1,3,5,2]oxadiazaborinin-9-ium-1-uide (2a)

Physical state: yellow solid. Melting point: 144–145 °C. Yield: 54%. NMR ^{1}H (400 MHz, $CDCl_3$): δ = 8.37- 8.35 (m, 3H, Ph and H-Py), 8.08 (t, *J* = 7 Hz, 1H-Py), 7.59 (t, *J* = 7 Hz, 1H-Py), 7.54 (d, *J* = 8 Hz, 1H-Py), 7.48 (t, *J* = 8 Hz, 2H, Ph), 7.38 (t, *J* = 7 Hz, 1H-Py). NMR ^{13}C (100 MHz, $CDCl_3$): δ = 165.7 (C-3), 154.6 (C-4a), 143.8 (C-Py), 138.6 (C-Py), 133.2 (C-Ph), 132.3 (C-Ph), 129.6 (C-Ph), 128.4 (C-Ph), 123.5 (C-Py) 120.5 (C-Py). NMR ^{19}F (564 MHz, $CDCl_3$): δ = -138.52 (q, $^1J_{B\text{-}F}$ = 14 Hz) (BF_2). NMR ^{11}B (192 MHz, $CDCl_3$): δ (ppm): 0.59 (t, $^1J_{B\text{-}F}$ = 13 Hz). GC–MS (EI, 70 (eV): m/z (rel.int.) 246 (78) $[M]^+$, 245 (100) $[M - H]^+$, 227 (5) $[M - F]^+$, 169 (1) $[M - C_6H_5]^+$. Anal. Calcd. for $C_{12}H_9BF_2N_2O$: C, 58.58; H, 3.69; N, 11.39. Found: C,58.76; H, 3.92 ; N,11.16.

1,1-difluoro-3-(*p*-tolyl)-1*H*-pyrido[1,2-*c*][1,3,5,2]oxadiazaborinin-9-ium-1-uide (2b)

Physical state: white solid. Melting point: 184–186 °C. Yield: 58%. NMR ^{1}H (400 MHz, $CDCl_3$) : δ = 8.36 (d, *J* = 5 Hz, 1H-Py), 8.26 (d, *J* = 8 Hz, 2H-Ph), 8.07 (t, *J* = 8 Hz, 1H-Py), 7.50 (d, *J* = 8 Hz, 1H-Py), 7.36 (t, *J* = 7 Hz, 1H-Py), 7.31 (d, *J* = 8 Hz, 2H-Ph), 2.46 (s, 3H- CH_3). NMR ^{13}C (100 MHz, $CDCl_3$): δ = 165.7 (C-3), 154.6 (C-4a), 144.2 (C-Py), 143.7 (C-Py), 138.5 (C-Py), 129.7 (C-Ph), 129.5 (C-Ph), 129.2 (C-Ph), 123.4 (C-Py), 120.3 (C-Py) 21.8 (C- CH_3). NMR ^{19}F (564 MHz, $CDCl_3$): δ = -138.68 (q, $^1J_{B\text{-}F}$ = 14 Hz) (BF_2). NMR ^{11}B (192 MHz, $CDCl_3$): δ = 0.56 (t, $^1J_{B\text{-}F}$ = 13 Hz). GC–MS (EI, 70 (eV): m/z (rel.int.) 259 (55) $[M - H]^+$, 241 (6) $[M - F]^+$, 91 (100) $[M - C_6H_4BF_2N_2O]^+$. Anal. Calcd. for $C_{13}H_{11}BF_2N_2O$: C, 60.04; H, 4.26; N, 10.77. Found:t C,58.98 ; H, 4.18; N,10.59.

3-(4-(dimethylamino)phenyl)-1,1-difluoro-1*H*-pyrido[1,2*c*][1,3,5,2]oxadiazaborinin-9-ium-1-uide (2c)[14]

Physical state: yellow solid (orange powder).[14] Melting point: 165–168 °C (Mp 167–169 °C).[14] Yield: 52 %. NMR ^{1}H (400 MHz, $CDCl_3$) δ = 8.25 – 8.22 (m, 2H-Ph), 7.97 (t, *J* = 7 Hz, 1H-Py), 7.40 (d, *J* = 7 Hz, 1H-Py), 7.23 (t, *J* = 7 Hz, 1H-Ph), 6.70 (d, *J* = 8 Hz, 2H-Ph), 3.09 (s, 6H- CH_3). NMR ^{13}C (100 MHz, $CDCl_3$): δ = 166.1 (C-3), 155.2 (C-4a), 153.9 (C-Ph), 142.9 (C-Py), 138.1 (C-Py), 131.7 (C-Ph), 131.1 (C-Ph), 123.0 (C-Py), 118.8 (C-Py), 110.9 (C-Ph) 39.9 (C- CH_3). NMR ^{19}F (564 MHz, $CDCl_3$): δ = - 139.58 (q, $^1J_{B\text{-}F}$ = 14 Hz) (BF_2). NMR ^{11}B (192 MHz, $CDCl_3$): δ = 0.51 (t, $^1J_{B\text{-}F}$ = 13 Hz). GC–MS (EI, 70 (eV): m/z (rel.int.) 289 (81) $[M]^+$, 288 (58) $[M - H]^+$, 148 (100) $[M - C_6H_4BF_2N_2O]^+$. Anal. Calcd. for $C_{14}H_{14}BF_2N_3O$: C, 58.17; H, 4.88; N, 14.54. Found: C, 58.08; H, 4.70 ; N,14.88.

1,1-difluoro-3-(4-nitrophenyl)-1*H*-pyrido[1,2-*c*][1,3,5,2]oxadiazaborinin-9-ium-1-uide (2d)

Physical state: yellow solid. Melting point: 198–202 °C. Yield: 70 %. NMR ^{1}H (400 MHz, $CDCl_3$) δ = 8.54 (d, *J* = 8 Hz, 2H-Ph), 8.46 (m, 1H-Py), 8.34 (d, *J* = 8 Hz, 2H-Ph), 8.20 (t, *J* = 7 Hz, 1H-Py), 7.62 (d, *J* = 8 Hz, 1H-Py), 7.52 (t, *J* = 7 Hz, 1H-Py). NMR ^{13}C (100 MHz, $CDCl_3$): δ = 163.2 (C-3), 153.9 (C-4a), 150.6 (C-Ph), 144.3 (C-Py), 139.1 (C-Py), 137.9 (C-Ph), 130.5 (C-Ph), 128.9 (C-Ph) 123.5 (C-Py), 121.7 (C-Py). NMR ^{19}F (564 MHz, $CDCl_3$): δ = -137.98 (q, $^1J_{B\text{-}F}$ = 13 Hz) (BF_2). NMR ^{11}B (192 MHz, $CDCl_3$): δ = 0.56 (t, $^1J_{B\text{-}F}$ = 13 Hz). GC–MS (EI, 70 (eV): m/z (rel.int.) 291 (100) $[M]^+$, 272 (5) $[M - F]^+$, 150 (69) $[M - C_6H_4BF_2N_2O]^+$. Anal. Calcd. for $C_{12}H_8BF_2N_3O_3$: C, 49.53; H, 2.77; N, 14.44. Found: C, 49.53; H, 2.88; N, 14.25.

1,1-difluoro-3-(naphthalen-2-yl)-1*H*-pyrido[1,2-*c*][1,3,5,2]oxadiazaborinin-9-ium-1-uide (2e)

Physical state: yellow solid. Melting point: 200–202 °C. Yield: 64 %. NMR ^{1}H (400 MHz, $CDCl_3$) δ = 8.94 (s, 1H- naph), 8.41 – 8.38 (m, 2H- Py and Naph), 8.13 (t, *J* = 7 Hz, 1H-Py), 8.02 (d, *J* = 7 Hz, 1H-Py), 7.92 (t, *J* = 7 Hz, 1H-Naph), 7.64 – 7.65 (m, 1H-Naph), 7.43 (t, *J* = 7 Hz, 1H-Py). NMR ^{13}C (100 MHz, $CDCl_3$): δ = 165.6 (C-3), 154.5 (C-4a), 143.9 (C-Py), 138.7 (C-Py), 135.8 (C-

View Article Online
DOI: 10.1039/C7NJ04032F

Naph), 132.6 (C- Naph), 131.3 (C-Naph), 129.6 (C-Naph), 128.5 (C-Naph) 128.1 (C-Naph), 127.9 (C-Naph), 126.7 (C-Naph), 125.1 (C-Naph), 123.6 (C-Py), 120.7 (C-Py) .NMR ^{19}F (564 MHz, $CDCl_3$): δ = - 138.53 (q, $^1J_{B\text{-}F}$ = 14 Hz) (BF_2). NMR ^{11}B (192 MHz, $CDCl_3$): δ = 0.64 (t, $^1J_{B\text{-}F}$ = 13 Hz).GC–MS (EI, 70 (eV): m/z (rel.int.) 296 (32) $[M]^+$, 127 (100) $[M - C_6H_4BF_2N_2O]^+$. Anal. Calcd. for $C_{16}H_{11}BF_2N_2O$: C, 64.91; H, 3.74; N, 9.46. Found: C, 64.72; H, 3.70; N, 9.88.

1,1-difluoro-3-(thiophen-2-yl)-1*H*-pyrido[1,2-*c*][1,3,5,2]oxadiazaborinin-9-ium-1-uide (2f)

Physical state: yellow solid. Melting point: 142–145 °C. Yield: 51 %. NMR ^{1}H (400 MHz, $CDCl_3$) δ = 8.33 (s, 1H-Py), 8.07 - 8.03 (m, 2H-Py and Thienyl), 7.64 (d, *J* = 5 Hz, 1H- Thienyl), 7.46 (d, *J* = 8 Hz, 1H-Py), 7.35 (t, *J* = 7 Hz, 1H-Py), 7.15 (t, *J* = 4 Hz, 1H-Thienyl). NMR ^{13}C (100 MHz, $CDCl_3$): δ = 161.8 (C-3), 154.5 (C-4a), 143.7 (C-Py), 138.7 (C-Py), 136.7 (C- Thienyl), 133.8 (C-Thienyl), 133.7 (C- Thienyl), 128.4 (C- Thienyl), 123.2 (C-Py), 120.2 (C-Py). NMR ^{19}F (564 MHz, $CDCl_3$): δ = - 139.05 (q, $^1J_{B\text{-}F}$ = 13 Hz) (BF_2). NMR ^{11}B (192 MHz, $CDCl_3$): δ = 0.37 (t, $^1J_{B\text{-}F}$ = 13 Hz). GC–MS (EI, 70 (eV): m/z (rel.int.) 252 (68) $[M]^+$, 233 (5) $[M - F]^+$, 111 (100) $[M - C_6H_4BF_2N_2O]^+$.
Anal. Calcd. for $C_{10}H_7BF_2N_2OS$: C, 47.65; H, 2.80; N, 11.11. Found: C,47.95; H, 2.75; N,11.01.

Conflicts of interest

There are no conflicts to declare.

Acknowledgments

The authors thank the Coordination for Improvement of Higher Education Personnel (CAPES) for the fellowships, and the National Council for Scientific and Technological Development (CNPq) for financial support (Process numbers 306.883/2015-5 and 402.075/2016-1 CNPq/Universal).

Supplementary material

Supplementary material associated with this article can be found, in the online version, at…

References and notes

1 C. Glotzbach, U. Kauscher, J. Voskuhl, N. S. Kehr, M. C. A. Stuart, R. Fröhlich, H. J. Galla, B. J. Ravoo, K. Nagura, S. Saito, S. Yamaguchi and E. U. Würthwein. *Org. Chem*., 2013, **78**, 4410.
2 L. S. Hung and C. H. Chen, *Mater. Sci. Eng. R.,* 2002, **39**, 143.
3 A. Mishra and P. Buerle, *Angew. Chem.,* 2012, **124**, 2060.
4 Y.-L. Rao and S. Wang, *Inorg. Chem.,* 2011, **50**, 12263.
5 R. Ziessel and A. Harriman, *Chem. Commun*., 2011, **47**, 611.
6 A. Harriman, L. J. Mallon, K. J. Elliot, A. Haefele, G. Ulrich and R. Ziessel, *J. Am. Chem. Soc*., 2009, **131**, 13375.
7 G. Ulrich, S. Goeb, A. De Nicola, P. Retailleau and R. Ziessel, *J. Org. Chem.,* 2011, **76**, 4489.
8 D. Frath, J. Massue, G. Ulrich and R. Ziessel, *Angew. Chem.,* 2014, **53**, 2290.
9 E. Okutan, S. O. Tumay and S. Yeşilot, *J Fluoresc.,* 2016, **6**, 2333.
10 V. I. Martynov, A. A. Pakhomov, N. V. Popova, I. E. Deyev, and A. G. Petrenko, *Acta Naturae*, 2016, **4**, 33.
11 A. Kamkaew, S. H. Lim, H. B. Lee, L. V. Kiew, L. Y. Chungc and K. Burgess, *Chem. Soc. Rev*., 2013, **1**, 77.
12 D. Dziuba, P. Jurkiewicz, M. Cebecauer, M. Hof and M. Hocek, *Angew. Chem.,* 2016, **55**, 174.
13 K. Jurek, J. Kabatc and K. Kostrzewska, *Color. Technol.,* 2017, **133**, 170.
14 A. M. Grabarz, A. D. Laurent, B. Jędrzejewska, A. Zakrzewska, D. Jacquemin, and B. Osmiałowski, *J. Org. Chem*., 2016, **81**, 2280.
15 J. Bednarska, R. Zalesny, M. Wielgus, B. Jedrzejewska, R. Puttreddy, K. Rissanen, W. Bartkowiak, H. Ågren and B. Osmiałowski, *Phys. Chem. Chem. Phys*., 2017, **19**, 5705.
16 E. S. Devi, A. Alanthadka, A. Tamilselvi, S. Nagarajan, V. Sridharana and C. U. Maheswaria, *Org. Biomol. Chem*., 2016, **35**, 8228.
17 H.G. Bonacorso, T. P. Calheiro, B. A. Iglesias, I. R. C. Berni, E. N. da Silva Júnior, J. B. T. Rocha, N. Zanatta and M. A. P. Martins, *Tetrahedron Lett*., 2016, **57**, 5017.
18 Y-Y. Wu, Y. Chen, G-Z. Gou, W-H. Mu, X. J. Lv, M. L. Du and W-F Fu, *Org. Lett*., 2012, **20**, 5226.
19 X. Xie, Y. Yuan, R. Krüger and M. Bröring, *Magn. Reson. Chem.,* 2009, **47**, 1024.
20 The crystallographic data for the structure of **2b** have been deposited with the Cambridge Crystallographic Data Centre and allocated the deposition number CCDC 1529635. Copies of the data can be obtained free of charge, on application to CCDC, 12 Union Road, Cambridge CB2 1EZ, UK (fax: +44 1223336033 or deposit@ccdc.com.ac.uk).
21 S. Hachiya, T. Inagaki, D. Hashizume, S. Maki, H. Niwa and T. Hirano, *Tetrahedron Lett*., 2010, **51**, 1613.
22 A. Harriman, L. J. Mallon, G. Ulrich and R. Ziessel, *ChemPhysChem.,* 2007, **8**, 1207.
23 K. Krumova, G. Cosa, *J. Am. Chem. Soc.,* 2010, **132**, 17560.
24 J. Bartelmess, W. W. Weare, N. Latortue, C. Duongb and D. S. Jones, *New J. Chem*., 2013, **37**, 2663.
25 Gaussian 09, Revision A.02, M. J. Frisch, G. W. Trucks, H. B. Schlegel, G. E. Scuseria, M. A. Robb, J. R. Cheeseman, G. Scalmani, V. Barone, G. A. Petersson, H. Nakatsuji, X. Li, M. Caricato, A. Marenich, J. Bloino, B. G. Janesko, R. Gomperts, B. Mennucci, H. P. Hratchian, J. V. Ortiz, A. F. Izmaylov, J. L. Sonnenberg, D. Williams-Young, F. Ding, F. Lipparini, F. Egidi, J. Goings, B. Peng, A. Petrone, T. Henderson, D. Ranasinghe, V. G. Zakrzewski, J. Gao, N. Rega, G. Zheng, W. Liang, M. Hada, M. Ehara, K. Toyota, R. Fukuda, J. Hasegawa, M. Ishida, T. Nakajima, Y. Honda, O. Kitao, H. Nakai, T. Vreven, K. Throssell, J. A. Montgomery, Jr., J. E. Peralta, F. Ogliaro, M. Bearpark, J. J. Heyd, E. Brothers, K. N. Kudin, V. N. Staroverov, T. Keith, R. Kobayashi, J. Normand, K. Raghavachari, A. Rendell, J. C.

View Article Online
DOI: 10.1039/C7NJ04032F

Burant, S. S. Iyengar, J. Tomasi, M. Cossi, J. M. Millam, M. Klene, C. Adamo, R. Cammi, J. W. Ochterski, R. L. Martin, K. Morokuma, O. Farkas, J. B. Foresman, and D. J. Fox, Gaussian, Inc., Wallingford CT, 2016.

26 B. K. Paul and N. Guchhait, *Photochem. Photobiol. Sci.*, 2011, **10**, 980.

27 Bruker, APEX2, SAINT, SADABS and XSHELL. Bruker AXS Inc., Madison, Wisconsin, USA,2010.

28 SHELX: G. M. Sheldrick, *Acta Cryst*., 2008, **A64**, 112–122.

29 P. Coppens, L. Leiserowitz and D. Rabinovich, *Acta Crystallogr.,* 1965, **18**, 1035.

30 G. Heinrich, S. Schoof and H. Gusten, *J. Photochem.*, 1974, **3**, 315.

31 R. R. Gagne, C. A. Koval, and G. C. Lisensky, *Inorg. Chem.*, 1980, **19**, 2854.

32 A. Bujacz, *Acta Crystallogr., Sect. D.* 2012, **68**, 1278.

33 E. F. Pettersen, T. D. Goddard, C. C. Huang, G. S. Couch, D. M. Greenblatt, E. C. Meng, and T. E. Ferrin, *J. Comput. Chem*., 2004, **25**, 1605.

34 M. D. Hanwell, D. E. Curtis, D. C. Lonie, T. Vandermeersch, E. Zurek and G. R. Hutchison, *J. Cheminform*., 2012, **4**, 1.

35 J. J. P. Stewart, *J. Mol. Mod*., 2007, **13**, 1173.

36 J. J. P. Stewart, Stewart Computational Chemistry. Colorado Springs, CO, USA. http://OpenMOPAC.net

37 G. M. Morris, R. Huey, W. Lindstrom, M. F. Sanner, R. K. Belew, D. S. Goodsell and A. J. Olson, *J. Comput. Chem*., 2009, **30**, 2785.

38 O. Trott and A. J. Olson, *J. Comput. Chem*., 2010, **31**, 455.

39 Dassault Systèmes BIOVIA, Discovery Studio Modeling Environment, Release 2017, San Diego: Dassault Systèmes, 2016.

View Article Online
DOI: 10.1039/C7NJ04032F

New fluorinated pyridine-based boron heterocycles showing optical properties were easy prepared and fully characterized. BSA-binding and molecular docking studies indicated strong interactions with the tryptophan site.